Received: 31 October 2024 | Revised: 10 March 2025 | Accepted: 17 March 2025

DOI: 10.1111/azo.12548

ORIGINAL ARTICLE

Acta Zoologica WILEY

Morpho-functional analysis of musculature and nervous system of mantle in brachiopod *Hemithiris psittacea* (Gmelin, 1791)

Anna V. Ratnovskaya[1,2] | **Tatyana V. Kuzmina**[1] | **Vladislav S. Kuzmin**[1,2]

[1]Biological Faculty, Moscow State University, Moscow, Russia

[2]Laboratory of Cardiac Electrophysiology, National Medical Research Cardiological Complex (NMRCC), Institute of Experimental Cardiology, Moscow, Russia

Correspondence
Anna V. Ratnovskaya, Biological Faculty, Moscow State University, Moscow 119234, Russia.
Email: belka190199@gmail.com

Funding information
Russian Science Foundation, Grant/Award Number: 23-14-00020

Abstract

The brachiopod mantle, which has a row of setae along its edge, plays a crucial role in environmental interactions and defence reflexes, triggering rapid valve closure. However, the organization of the muscular and nervous systems in the mantle of rhynchonelliform brachiopods, as well as the sensory mechanisms of the mantle setae, remains largely unexplored. In this study, we present a morpho-functional analysis of the neuromuscular system of the mantle in the brachiopod *Hemithiris psittacea,* using transmission electron microscopy, immunocytochemistry, and in vivo video recordings of mantle movements. The mantle contains numerous thin muscles extending from its central region to the periphery, but not reaching the mantle edge. The contraction of these muscles allows the mantle with setae to retract into the mantle cavity. Additionally, the mantle is innervated by numerous radial nerves that connect to the marginal mantle nerve. We demonstrate that mantle contraction may occur independently of the central nervous system. However, the subenteric ganglion plays a role in maintaining the mantle in a pre-contracting state during rest, thus enhancing the sensory selectivity of the setal sensory complexes.

KEYWORDS

Brachiopoda, mantle, morpho-functional analysis, muscles, nervous system, seta, ultrastructure

1 | INTRODUCTION

Brachiopoda is a phylum of benthic marine invertebrates characterized by a long and well-documented paleontological history (Carlson, 2016). The soft body of brachiopods is protected by a bivalve shell and is usually attached to the substrate by a pedicle. The phylum Brachiopoda includes three subphyla: Linguliformea, Craniiformea, and Rhynchonelliformea (Williams et al., 1996). Recent rhynchonelliform and craniiform brachiopods have calcareous shells and lecithotrophic larvae, whereas recent linguliforms have organophosphatic shells and planktotrophic juveniles (Lüter, 2007; Malakhov et al., 2021). Furthermore, rhynchonelliform brachiopods exhibit articulatory structures that connect the valves and possess calcareous support for the tentacle organ, the lophophore. These articulatory and support structures are absent in both craniiforms and linguliforms.

In all brachiopods, the soft body occupies the posterior space within the shell, and the body wall forms a mantle that lines the inner surfaces of the valves. The mantle cavity, enclosed by the mantles, contains the lophophore, which is primarily used for filtering food particles and respiration (Rudwick, 1970). The mantle

consists of inner and outer epithelia, with the inner epithelium transitioning into the outer epithelium at the mantle edge. This transition zone at the mantle edge forms a mantle groove. The mantle groove separates the mantle into the outer mantle lobe, which is located under the shell, and the inner mantle lobe, which lines the mantle cavity. The outer epithelium underlies and produces the shell, while the inner ciliated epithelium cleans the mantle cavity of unwanted particles and regulates water flow. Setae are located along the mantle edge, serving primarily as sensory structures (Rudwick, 1970). During filtration, the valves of the brachiopod shell are slightly open, allowing the setae to extend beyond the mantle cavity. Mechanical stimulation of sensitive elements at the mantle edge triggers contractions of the mantle and leads to the closure of the shell valves (Rudwick, 1970).

Despite significant advances in understanding brachiopod biology, the organization of the muscular and nervous systems of the mantle in rhynchonelliform brachiopods, as well as the mechanisms underlying the sensory function of the mantle setae, have remained largely unknown. In this study, we present a morpho-functional analysis of the muscular and nervous systems of the mantle in the brachiopod *Hemithiris psittacea* (Gmelin, 1791), using a set of different methods, such as transmission electron microscopy, confocal laser scanning microscopy with immunocytochemistry, and in vivo video recording of mantle movements.

2 | MATERIALS AND METHODS

2.1 | Animals

Thirty specimens of *H. psittacea* were collected by diving at a depth of 9 m in August 2021 at the White Sea Biological Station of Moscow State University (Kandalakshskii Bay, White Sea; 66.33184, 33.74719). We studied 10 small specimens with dorsal valve lengths of up to 2 mm and 20 large specimens with dorsal valve lengths of up to 16 mm (Figure 1a).

2.2 | Microscopy

The animals were relaxed in 2.7% $MgCl_2$ for 30 min. The large specimens were then dissected to obtain preparations of the mantle (volume 3–5 mm^3).

For transmission electron microscopy (TEM), two whole small specimens (dorsal valve lengths 0.8 and 1 mm) and two dorsal mantle preparations from large brachiopods (dorsal valve length 12 and 15 mm) were fixed in 2.5% phosphate-buffered glutaraldehyde (pH 7.2) with sucrose for 3 h at 4°C. The material was then rinsed in the same buffer. After postfixation in 1% phosphate-buffered osmium tetroxide with sucrose for 1 h at 20°C, the material was rinsed in distilled water. Next, the whole small specimens were decalcified in 7% EDTA in distilled water (pH 7.5) for 1 h at room temperature

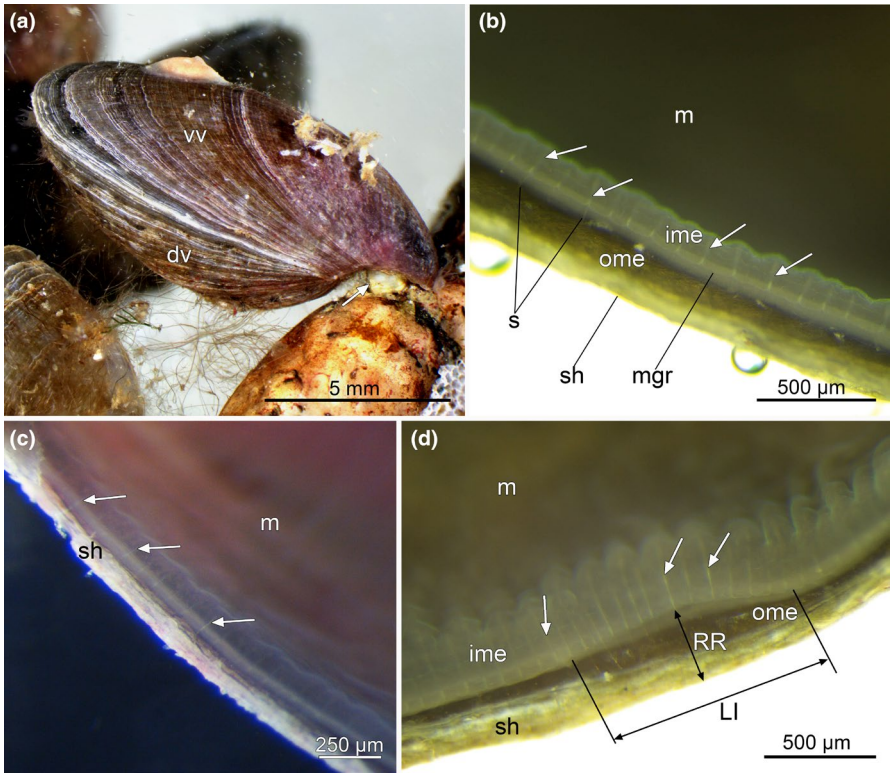

FIGURE 1 View and the mantle edge during the functional experiments on the brachiopod *Hemithiris psittacea* (light microscopy). (a) A specimen attached to the substratum, arrow shows the pedicle; (b) mantle edge immediately after preparation; (c) mantle edge after relaxation; (d) mantle edge after local mechanical impact: dv, dorsal valve; ime, inner mantle epithelium; LI, lateral irradiation; m, mantle; mgr, mantle groove; ome, outer mantle epithelium; RR, retractive response; s, setae; sh, shell; vv, ventral valve; arrows on (b)–(d) show setae follicles.

and then rinsed in distilled water. Afterward, all samples were dehydrated through an ascending ethanol series and embedded in resin (Low Viscosity Embedding Media, Spurr). Semithin sections (1 μm thick) were cut with a glass knife on a Leica EM UC6 ultramicrotome (Leica Microsystems GmbH, Wetzlar, Germany) and stained with methylene blue, and then examined and photographed using a Zeiss Axioplan 2 imaging photomicroscope. Ultrastructure was studied on ultrathin silver sections (65–75 nm thick). Ultrathin sections were cut with a diamond knife on a Leica EM UC6 ultramicrotome, then mounted on copper grids, stained with uranyl acetate (0.5%) and lead citrate (0.4%), and examined with Jeol Jem 100 V and Jeol-1011 80 kV transmission electron microscopes (JEOL Ltd., Tokyo, Japan).

For confocal laser scanning microscopy (CLSM), three small specimens (with dorsal valve lengths ranging from 1.6 to 2 mm) and the mantle preparations of two large specimens (with dorsal valve lengths of 12 and 16 mm) were fixed overnight in a 4% paraformaldehyde solution in phosphate buffer (pH 7.4) (Fisher Scientific, Pittsburgh, PA, USA). The samples were then washed three times for 15 min each in phosphate buffer (pH 7.4). Non-specific binding sites were blocked with 10% BSA (Sigma A2153) in the same buffer containing 2% Triton X-100 (Fisher Scientific) (PBT). The samples were incubated with the primary antibody in PBT: mouse anti-α-Tubulin was used at a dilution of 1:700 (Sigma SAB 4200776); rabbit anti-5HT at 1:5000 (Sigma S554); and rabbit anti-FMRF-amide at 1:2500 (Sigma AB15348). Incubation lasted for 24 h at 4°C, followed by washing in PBT. The samples were then exposed to the secondary antibody: goat anti-mouse conjugated with Alexa-635 (1:1000); goat anti-rabbit conjugated with Alexa-546 (1:1000); ThermoFisher Scientific in PBT for 12 h at 4°C. Then, the specimens were washed in PBT and incubated with Phalloidin-FITC-495 (Sigma P5282, 1:100) and DAPI (Sigma D9542, 1:1000) for 2 h at room temperature in the dark. The material was subsequently washed in PBS three times for 20 min each, mounted on a cover glass, and embedded in glycerol. Specimens were examined with a Nikon Eclipse Ti confocal microscope (Moscow State University, Moscow, Russia). Z-projections were prepared using ImageJ version 1.43.3.

2.3 | Analysis of the contractile responses of the mantle edge

The registration and analysis of mantle contractile activity were performed on large brachiopods with a dorsal valve length of 14 ± 2 mm. The animals were placed in an experimental thermostabilized chamber (10°C) with a capacity of 300 mL filled with filtered seawater. The chamber was mounted on the stage of a Leica MZ6 stereo microscope (Leica Microsystems GmbH, Wetzlar, Germany). The peripheral portion of the ventral valve of the shell was gently removed using microsurgical instruments to expose the mantle edge. The removal of the shell edge resulted in a spontaneous, generalized contractile retraction of the inner lobe of the dorsal mantle and internalization of the setae of the dorsal mantle (Figure 1b). Therefore, all animals were allowed to adapt for 1 hour after the manipulation and before the experiments, which was sufficient to relax the dorsal mantle and expose the setae (Figure 1c).

In situ mantle contractions were induced by mechanical stimulation in six manipulated animals (Figure 1d). A localized mechanical stimulation of equal magnitude was applied consecutively (5 min) at five points on the mantle edge of each specimen (Figure 2a). For the stimulation, a device consisting of a micromotorized micromanipulator and a glass capillary with a smooth blunt tip, 50 μm^2 in

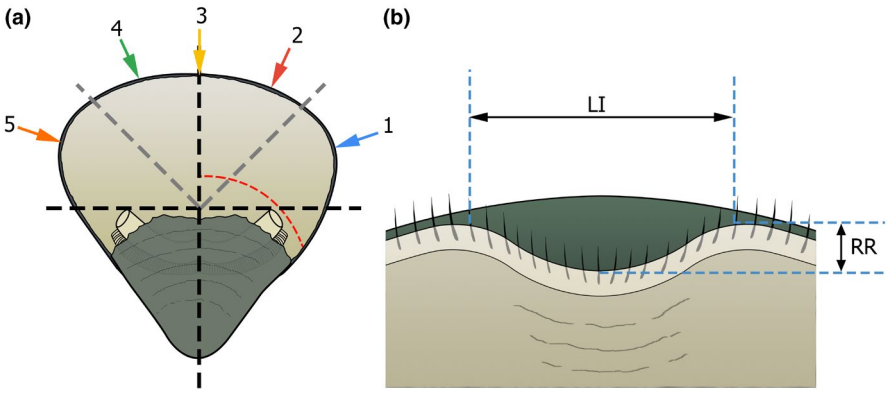

FIGURE 2 Schemes of the brachiopods during the registration of the contractile activity of the mantle (ventral valve is cut). (a) five sectors of mechanical impact; (b) retractive response and lateral irradiation of the mantle. Arrows show the point of mechanical impact, the red dotted line shows a hemicircular incision of the radial mantle nerves for denervation of the peripheral mantle. LI, lateral irradiation; RR, retractive response.

diameter, sealed with the aid of a microforge (Narishige, MF2, Japan), was used. The contractile responses of the mantle were recorded at 60 fps using a ToupCam UCMOS05100KPA camera (frame resolution 2560×1920 px) integrated into the optical scheme of a Leica MZ6 stereo microscope (Leica Microsystems GmbH, Wetzlar, Germany) (magnification 40×).

Before the stimulation, the distance between the shell margin and the edge of the inner mantle lobe was measured and assumed to be the rest distance (RD). The retractile responses (RR) were calculated as the distance from the shell margin to the edge of the inner mantle lobe at the point of mechanical stimulation at 5, 10, 15, 20, 25, 30, 40, 50, 60, 90, 120, 150, and 180 s after the stimulus application, with the RD subtracted (Figures 1c and 2b). Using the RR values, contraction-relaxation curves (CR curves) were reconstructed for each of the 5 points on the mantle edge where the mechanical stimulus was applied (Figure 2a). Also, the magnitude of the lateral irradiation (LI) of the retractile response was calculated as the length of the mantle edge exhibiting retraction of not less than 0.1 mm after stimulus application. RD, RR, and LI were calculated using ImageJ software.

In a separate series of experiments ($n=6$), denervation of the peripheral mantle was performed by cutting the radial nerves of the mantle. A hemicircular incision was made near the anterior body wall, as shown in Figure 2a. After a 1 h adaptation period, the experiments were carried out according to the same protocol as previously described for intact animals.

2.4 | Statistics

Statistical analysis was carried out using GraphPad Prism version 7. The normality of the groups was tested using the Shapiro–Wilks test where needed. Hypothesis testing was carried out using two-way ANOVA with further Sidak's post-hoc multiple comparisons where appropriate. The relaxation half-times were calculated based on the CR curves after exponential fitting and regression quality assessment using GraphPad Prism. The nonparametric Mann–Whitney (M–U) test was used for comparing half-relaxation times. A p-value of <0.05 was considered statistically significant. All results are expressed as means ± SD for n experiments.

3 | RESULTS

3.1 | Mantle anatomy

The brachiopod mantle is a long fold of the body wall that lines the inner surface of the valves. The mantle margin consists of inner and outer mantle lobes, which are continuous at the mantle groove along the shell edge (Figure 3). The inner mantle lobe is lined by an inner mantle epithelium, whereas the outer mantle lobe is lined by an outer mantle epithelium. Cells within the inner epithelium are characterized by microvilli and a single cilium, while cells of the outer epithelium lack both cilia and microvilli. Instead, they attach to the shell via hemidesmosomes (Figure 3). A layer of connective tissue lies between the basal laminae of the inner and outer epithelia. This connective tissue contains an extracellular matrix with amoebocytes and muscle cells. The extracellular matrix is traversed by mantle coelomic canals, which extend from the perivisceral coelom. Marginal setae emerge from the mantle groove at the mantle edge. Each seta is housed within a follicle, an invagination of the inner epithelium. The base of the follicle is formed by a large, specialized cell known as a setoblast, which produces the setal material. The cells that line the follicle attach to the surface of the setae via hemidesmosomes. Mantle nerves are

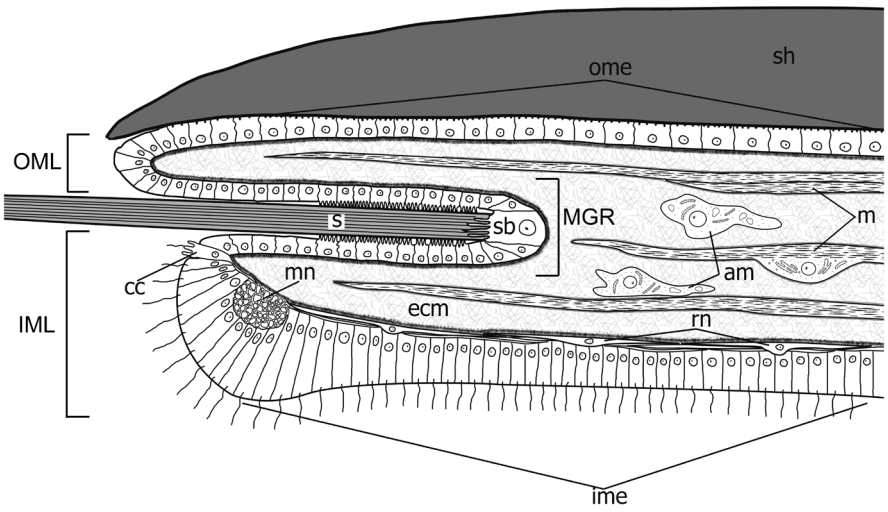

FIGURE 3 Scheme of the sagittal section of the mantle margin in *Hemithiris psittacea*. Am, amoebocytes; cc, collar cell; ecm, extracellular matrix; ime, inner mantle epithelium; IML, inner mantle lobe; m, muscles; MGR, mantle groove; mn, marginal nerve; ome, outer mantle epithelium; OML, outer mantle lobe; rn, radial nerves; s, setae; sb, setaeblast; sh, shell.

situated basiepithelially within the inner mantle epithelium (Figure 2).

3.2 | Mantle musculature

The muscular system of *H. psittacea* is well developed in both the dorsal and ventral mantles. It consists of serial mantle muscles that extend longitudinally from the central part of the mantle to its periphery but do not reach the mantle margin (Figures 3 and 4a,b). These muscles run along the basal part of the setal follicles but do not make direct contact with them (Figure 4b).

The serial mantle muscles are located within the connective tissue between the inner and outer epithelia (Figures 3 and 5a). They are rounded in cross-section with diameters ranging from 1.5 to 5 μm. Each muscle can be composed of two to three muscle cells (Figure 5a,c,g) or be formed by a single muscle cell (Figure 5f). In small specimens, the muscles are arranged in a single layer within the connective tissue (Figures 4a and 5a), while in large specimens, they are organized into several layers (Figures 4b and 5g).

In all specimens, mantle muscle cells exhibit a consistent structure, comprising a soma and long processes containing myofilaments. The soma contains a large, elongated nucleus (Figure 5a), several mitochondria (Figure 5b), numerous ribosomes, and a well-developed rough endoplasmic reticulum (Figure 5c,d). The muscle processes contain closely packed myofilaments, forming smooth muscle (Figure 5a,c,e–j). In transverse sections of these processes, the thick myofilaments vary in diameter: in small specimens, they measure approximately 65 nm at their thickest point, while in large specimens, they measure around 71 nm. Additionally, muscle cells contain canals of sarcoplasmic reticulum (Figure 5e) and vesicles with electron-lucent contents (Figure 5f).

Each mantle muscle is surrounded by a thin, electron-dense layer of extracellular matrix, resembling the basal lamina of the inner and outer mantle epithelia. Muscle cells are attached to this matrix by a series of hemidesmosomes (Figure 5a,g,h). We did not observe adherens junctions between muscle cells. The plasmalemma of the muscle cells may form finger-like projections into the extracellular matrix (Figure 5c,i).

Amoebocytes sometimes occur adjacent to muscle cells. These cells can reach up to 1.5 μm in diameter and extend long processes that envelop the muscle cells from all sides (Figure 5j). Amoebocytes are characterized by an electron-dense cytoplasm, a well-developed rough endoplasmic reticulum, and a high quantity of free ribosomes.

3.3 | Mantle nervous system

The dorsal and ventral mantles are innervated by a pair of main mantle nerves that originate from the subenteric ganglion. Within the mantle, these nerves branch into finer radial nerves that extend toward the mantle edge and connect with the marginal mantle nerve, which runs along the entire edge of the mantle and is situated at the base of the mantle groove (Figure 6a,d). The radial mantle nerves may exhibit varicosities (Figure 6b,d) and form very thin anastomoses (Figure 6c). The distal portions of the radial nerves extend near the setae follicles and do not connect with them.

The fine structure of mantle nerves is the same in large and small specimens. The radial and marginal mantle nerves are entirely situated within the inner mantle epithelium (Figure 7a), which is composed of monociliated supportive cells with narrow basal processes (Figure 7b). The apical surface of these cells contacts the mantle cavity and bears microvilli. The cell bodies are joined to each other by adherens junctions. The cytoplasm contains electron-dense granules, a well-developed rough endoplasmic reticulum, free ribosomes, and a nucleus surrounded by abundant mitochondria

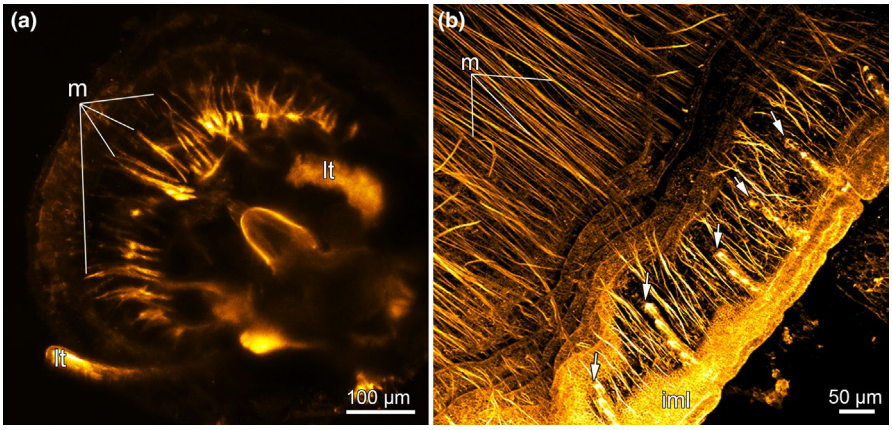

FIGURE 4 Organization of the mantle musculature in *Hemithiris psittacea*, Z-projections after staining with phalloidin, CLSM. (a) A small specimen after removal of the ventral valve. (b) A mantle edge of a large specimen. Iml, inner mantle lobe; m, muscles; lt, lophophore tentacle, arrows show setal follicles.

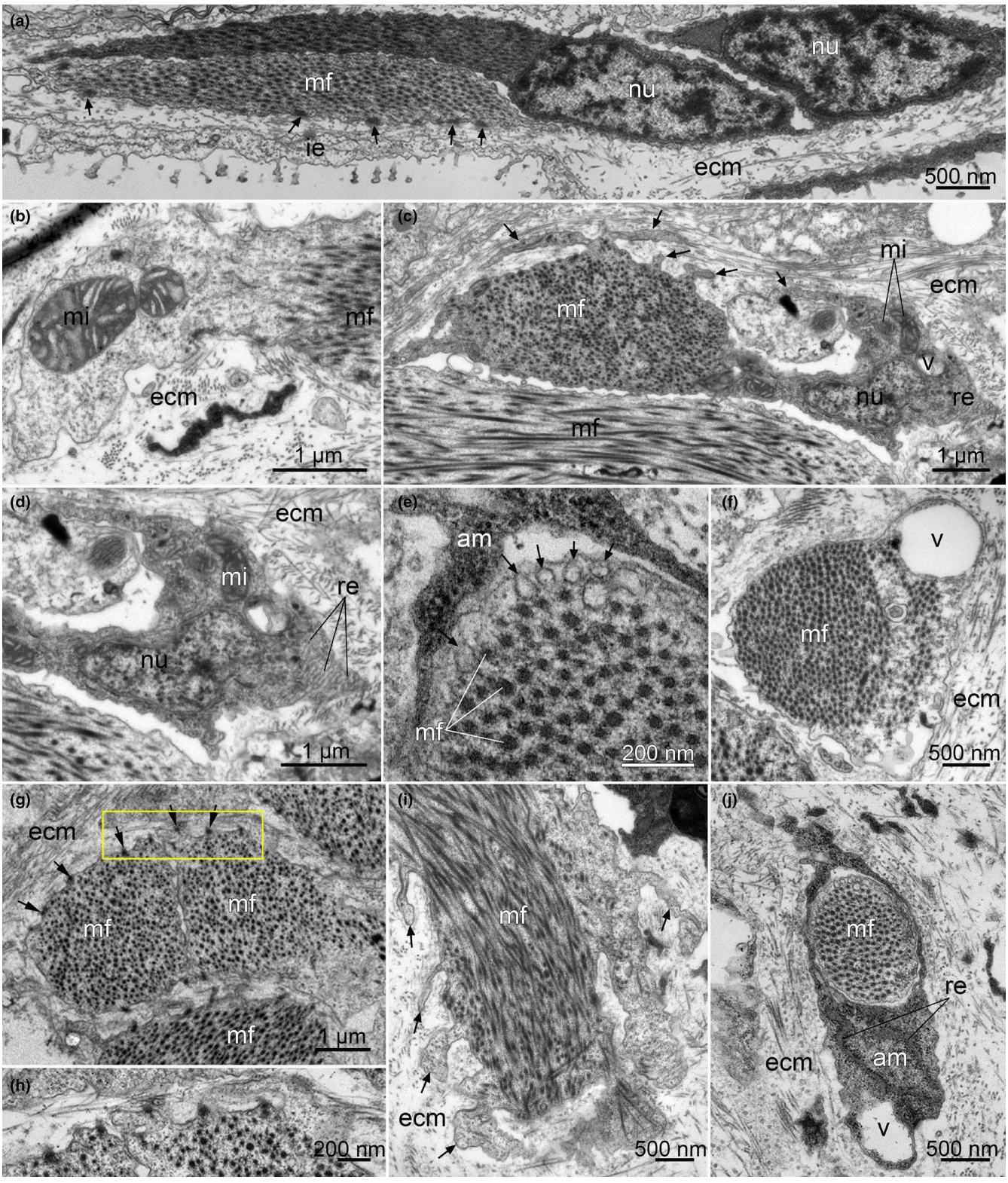

FIGURE 5 Fine structure of mantle muscle cells in *Hemithiris psittacea*, TEM. (a), small specimen, (b)-(j), large specimens. (a) Muscle cells arranged in a single layer, arrows show hemidesmosomes. (b) Soma of the muscle cell. (c) Muscle cell with finger-like projections (arrows). (d) Enlarged fragment of (c). (e) Part of muscle cell process with canals of sarcoplasmic reticulum (arrows). (f) Part of muscle cell process with a vesicle. (g) Muscle consisting two muscle cells, arrows show hemidesmosomes, yellow frame shows area in (h). (h) Hemidesmosomes and basal lamina-like structure around muscle cells. (i) Part of muscle cell process with finger-like projections (arrows). (j) Amoebocyte surrounding of the muscle cell. Am, amoebocyte; ecm, extracellular matrix; ie, inner epithelium cell; mf, myofilaments; mi, mitochondria; nu, nucleus; re, rough endoplasmic reticulum; v, vesicle with electron-lucent content.

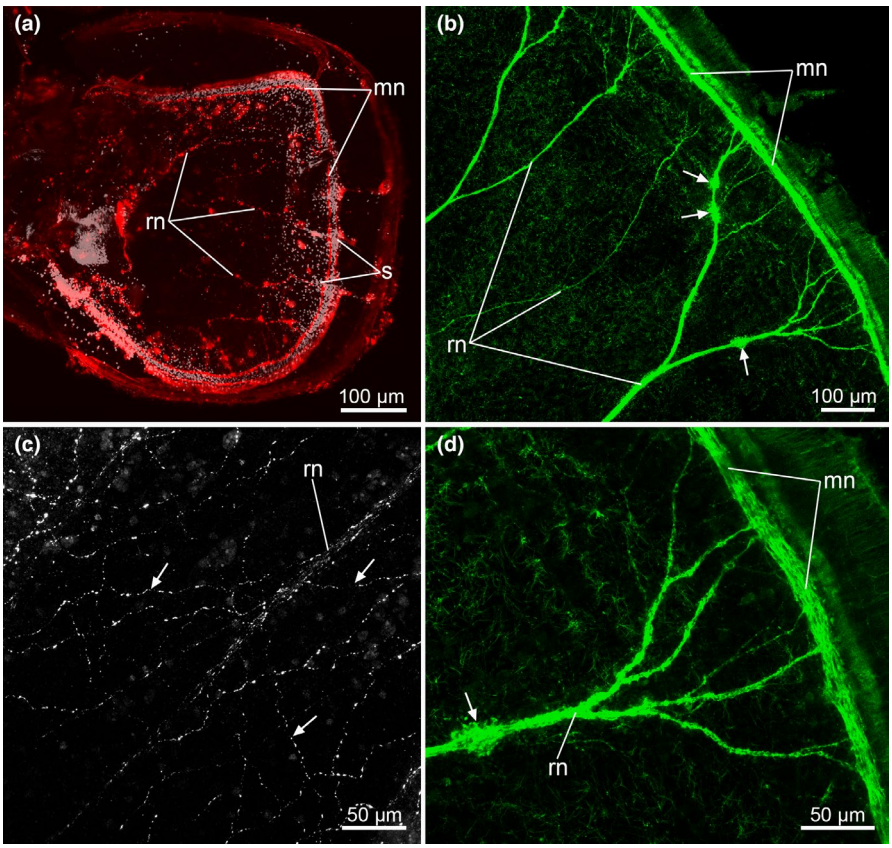

FIGURE 6 Organization of the nervous system in the mantle of *Hemithiris psittacea*, CLSM. (a) Dorsal mantle nervous system in a small specimen, Z-projection after double staining against 5-HT (red) and DAPI (grey). (b) Part of the mantle edge in a large specimen, Z-projection after staining against acetylated alpha-tubulin (green), arrows show varicosities in radial mantle nerves. (c) Part of the mantle in a large specimen, Z-projection after staining against FMRF-amide (grey), arrows show anastomoses between radial mantle nerves. (d) Enlarged region of (b). Mn, marginal mantle nerve; rn, radial mantle nerves; s, setae.

(Figure 7c,d). The narrow basal processes, containing intermediate filaments, are attached to the basal lamina via hemidesmosomes (Figure 7e). The proximal parts of the radial nerves, located near the main mantle nerves, and also the marginal nerve, are relatively large and are divided into several portions by the basal processes of supportive cells (Figure 7b,e).

The mantle nerves consist of two types of neurites. The first type is the most common, measuring up to 500 nm in diameter, with an electron-lucent cytoplasm, microtubules, and sparse dense-core vesicles (Figure 7a,e,f). The second type of neurites is larger, up to 1 µm in diameter, with an electron-dense cytoplasm containing both electron-lucent and dense-core vesicles (Figure 7f,h). In the proximal parts of the radial nerves, we observed large perikarya characterized by a large, irregularly shaped nucleus with a nucleolus. The cytoplasm of these perikarya is electron-lucent and contains mitochondria, rough endoplasmic reticulum, Golgi complexes, and several dense-core vesicles (Figure 7g).

The nerves, which contain both types of neurites and are surrounded by a basal lamina, are found within the connective tissue of the mantle (Figure 7h). Additionally, we observed rare radial nerves within the outer mantle epithelium, which also contain the two types of neurites (Figure 8a).

Transmission electron microscopy revealed that collar receptor cells are situated near each setae follicle (Figures 3 and 8b,c). These collar cells are monociliated, with the cilium surrounded by a collar composed of nine thick microvilli. The collar cells are connected to neighbouring cells of the inner mantle epithelium via adherens junctions. The microvilli of the collar are triangular in the transverse section, with their apexes facing inward (Figure 8b,c). The receptor cells have a large nucleus, and their cytoplasm contains electron-dense vesicles and Golgi complexes. The basal part of the receptor cells extends toward the mantle marginal nerve (Figure 8c).

4 | CONTRACTILE ACTIVITY OF THE MANTLE

Following the removal of the shell edge, a generalized contractile retraction of the mantle's inner lobe was observed, causing all setae to retract fully into the mantle cavity (Figure 1b). After an adaptation period, the mantle relaxed, allowing the setae to extend beyond the shell edge (Figure 1c). Additionally, mechanical stimulation induced retraction of the setae into the mantle cavity, indicative of the retractile response in this region (Figures 1d and 2b).

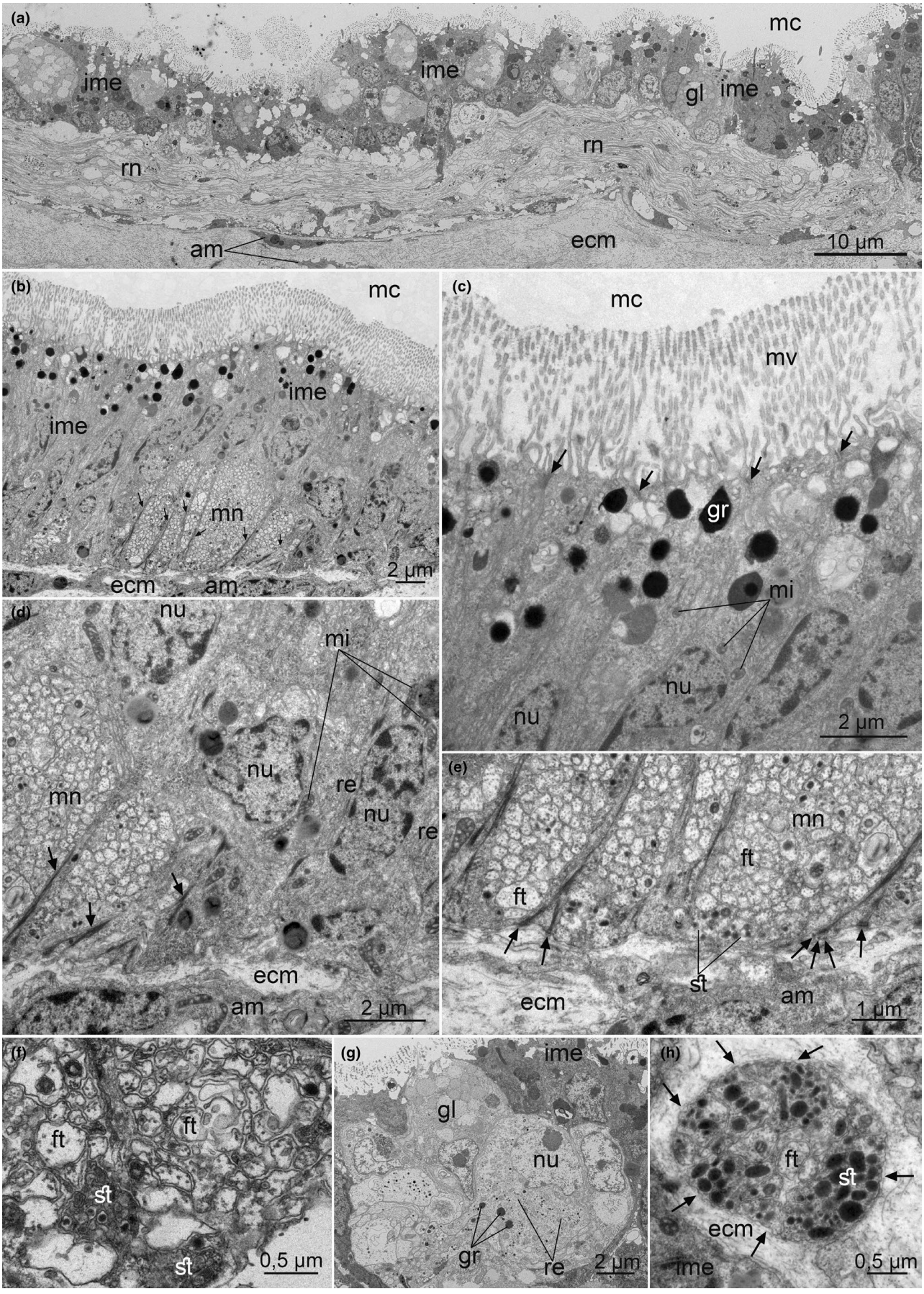

FIGURE 7 | Legend on next page.

FIGURE 7 Fine structure of the nervous system in the mantle of *Hemithiris psittacea*, TEM. (a) Longitudinal section of the proximal part of the radial mantle nerve. (b) Cross-section of the marginal mantle nerve, arrows show basal processes of supportive cells. (c) Apical part of supportive cells, arrows show adherens junctions. (d) Basal part of supportive cells, arrows show basal processes. (e) Basal processes of the supportive cells and neurites of the marginal mantle nerve, arrows show hemodesmosomes of supportive cells. (f) Cross-section of part of the marginal mantle nerve. (g) Perikarya of the radial mantle nerve. (h) Mantle nerve in the extracellular matrix, arrows show the basal lamina. Am, amoebocyte; ecm, extracellular matrix; ft., neurites of the first type; gl, glandular cell; gr, granule; ime, inner mantle epithelium; mc, mantle cavity; mi, mitochondria; mn, marginal mantle nerve; mv, microvilli; nu, nucleus; re, rough endoplasmic reticulum; rn, radial mantle nerve; st, neurites of the second type.

4.1 | Mantle edge retention

The position and the distance between the shell margin and the edge of the inner mantle lobe (rest distance, RD) were calculated before mechanical impact in intact or denervated animals. In all experiments, the entire mantle edge was retained inside the shell. The RD was less than 0.3 mm in all tested sectors in untreated animals (Figure 9). The RD varied insignificantly among mantle sectors, with the smallest RD in the lateral sector S5 (114.6 ± 20.8 µm, $n = 6$). However, denervation caused a relaxation of the mantle edge, resulting in a reduction of the mantle retention and a decrease of the RD. This effect was maximal for the anterior-lateral S2 sector of the mantle.

4.2 | Mechanically induced retractile responses of the mantle edge

Mechanically induced retractile responses of the mantle edge were analysed in intact and denervated animals. In our experiments, an application of a localized mechanical stimulus caused retractile responses (RR) that were restricted to a mantle sector and never resulted in a generalized retraction ($n > 30$) in either intact or denervated animals. The localized RR developed within seconds, reaching peak retraction 5 s after stimulation. After the peak, the retraction was followed by a slow (>100 s) relaxation of RR, exhibiting exponential decay (Figure 10a). The magnitude of RR in intact animals ranged from 160.6–233.5 µm, which is 1.5–2 times greater than the RD (Figure 10a). The peak value of RR and the relaxation rate varied insignificantly among sectors of the mantle (Figure 10b,c). Denervation potentiated RR, prolonged the retracted state, and delayed relaxation (Figure 10b). The duration of the time interval required for half-relaxation after RR increased more than twice in denervated animals (67.2 ± 33.6 vs. 168.5 ± 63 s, $n = 6$, Figure 10d,e).

As aforementioned, the mechanically induced retractile responses are localized. Nevertheless, the retraction revealed expansion beyond the area of stimulus administration along the mantle perimeter, characterized by a diminishing symmetrical lateral irradiation (LI) relative to the location of stimulation (Figures 1d and 2b). The retraction is maximal at the point of stimulation. LI varies among mantle sectors and animals but does not exceed 900 µm in our experiments with intact animals. The denervation augments LI; this parameter is significantly increased in the anterior-lateral sector S2 of the mantle (Figure 10f).

5 | DISCUSSION

5.1 | Organization of the mantle muscles

Our findings indicate that the mantle of *H. psittacea* contains numerous longitudinal smooth muscles, each composed of one or more cells. Similar mantle musculature has been documented in adult and juvenile brachiopods, as well as in larvae, where these appear as serially arranged muscles (Altenburger & Wanninger, 2009, 2010; Santagata, 2011).

There are observable differences in the arrangement of mantle muscles during brachiopod growth. In smaller specimens, the muscles are arranged in a single layer. However, as the brachiopods increase in size, the muscles start to develop multiple layers, likely due to the thickening of connective tissue in the mantle.

The mantle muscles of *H. psittacea* are surrounded by a thin layer of electron-dense extracellular matrix that resembles a basal lamina and therefore can have an epithelial origin (Figure 3). Based on this observation, we propose that the mantle muscles of brachiopods are extensions of the coelomic canals that extend into the extracellular matrix of the mantle.

Our data indicate that the thick myofilaments in the mantle muscles exhibit varying diameters, suggesting that these myofilaments are spindle-shaped, confirming the smooth nature of the mantle muscles. The maximum diameter of the thick myofilament is 71 nm, which is consistent with the data on the muscles of lophophore tentacles and in the smooth muscles of adductors in different brachiopod species (Kuga & Matsuno, 1988; Kuzmina & Temereva, 2021; Reed & Cloney, 1977;

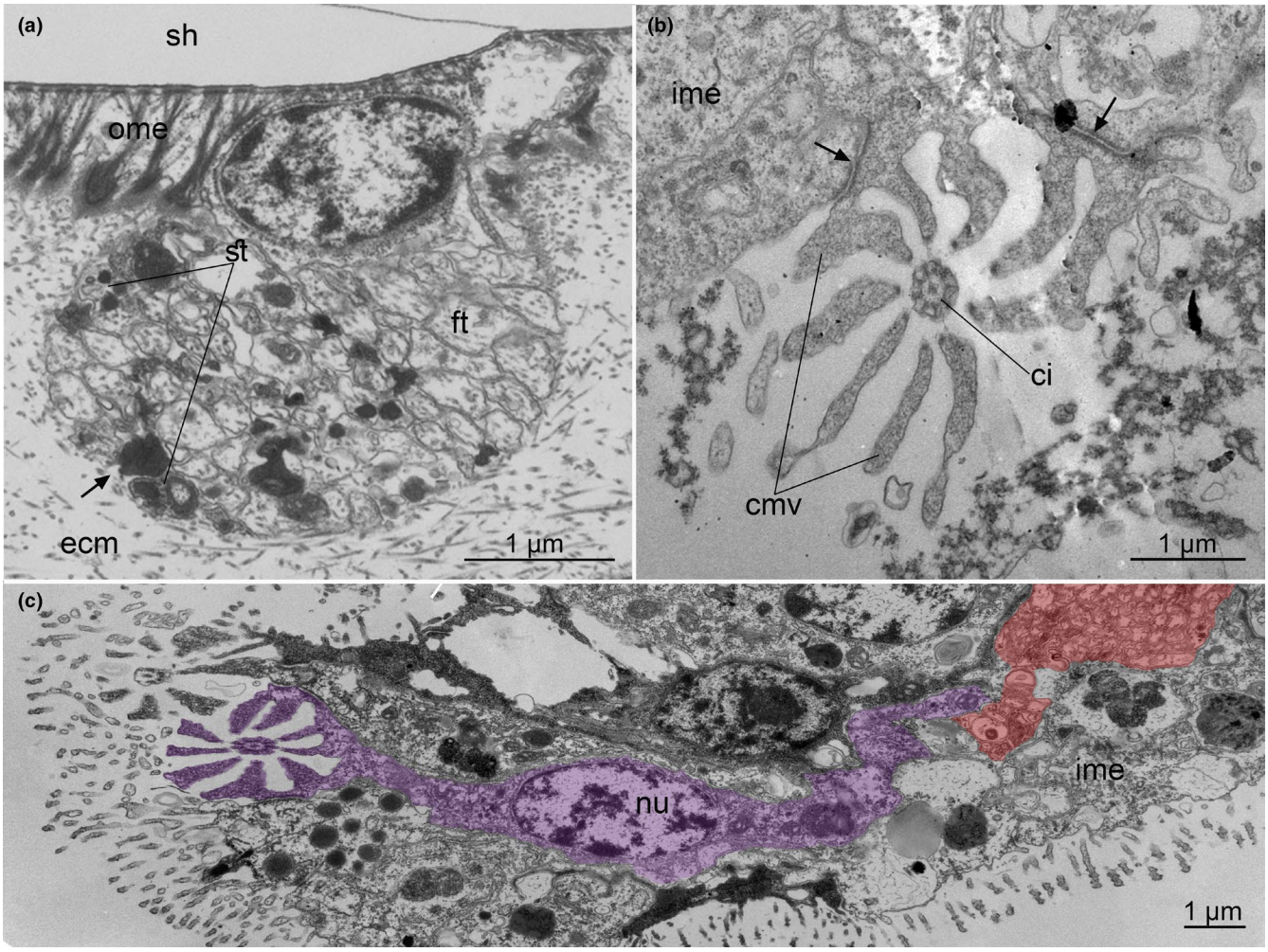

FIGURE 8 Fine structure of elements in the mantle nervous system of *Hemithiris psittacea*, TEM. (a) Nerve in the outer mantle epithelium, arrow shows the basal lamina. (b) Transverse section of apical part of collar receptor, arrows show zonula adherens. (c) Parasaggital section of the mantle edge, the collar receptor (violet) extends toward the marginal mantle nerve (red). Ci, cilium; cmv, microvilli of the collar receptor; ecm, extracellular matrix; ft., neurites of the first typr; ime, inner epithelium cell; nu, nucleus; ome, outer epithelium cell; sh, shell; st, neurites of the second type.

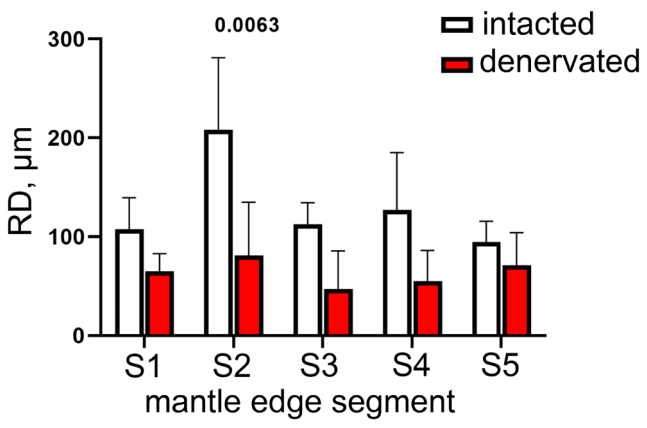

FIGURE 9 The distance between the shell margin and the edge of the inner mantle lobe (rest distance, RD) observed before mechanical stimulation in intact (transparent) and denervated (red) animals was calculated for each point (S1–S5) as shown in Figure 2a. Exact *p*-value (two-way ANOVA) is shown in the figure.

Storch & Welsch, 1976). This diameter suggests a high paramyosin content in the muscle fibres (Kuzmina & Temereva, 2021). We assume that the contraction of longitudinal mantle muscles causes the mantle to retract inside the shell, which is essential for valve closure in response to danger. The high paramyosin content in these smooth mantle muscles likely enables the mantle edge to remain retracted when the brachiopod valves are closed for a long time.

Our results indicate that the mantle muscles do not connect directly to the setal follicles, although they come close to them. Despite lacking muscles to control individual setae, brachiopods can retract the inner lobe of the mantle edge, aligning the setae parallel to the inner shell surface within the mantle cavity (Figure 11). Consequently, mantle muscle contraction causes the setae to retract inward into the mantle cavity during valve closure.

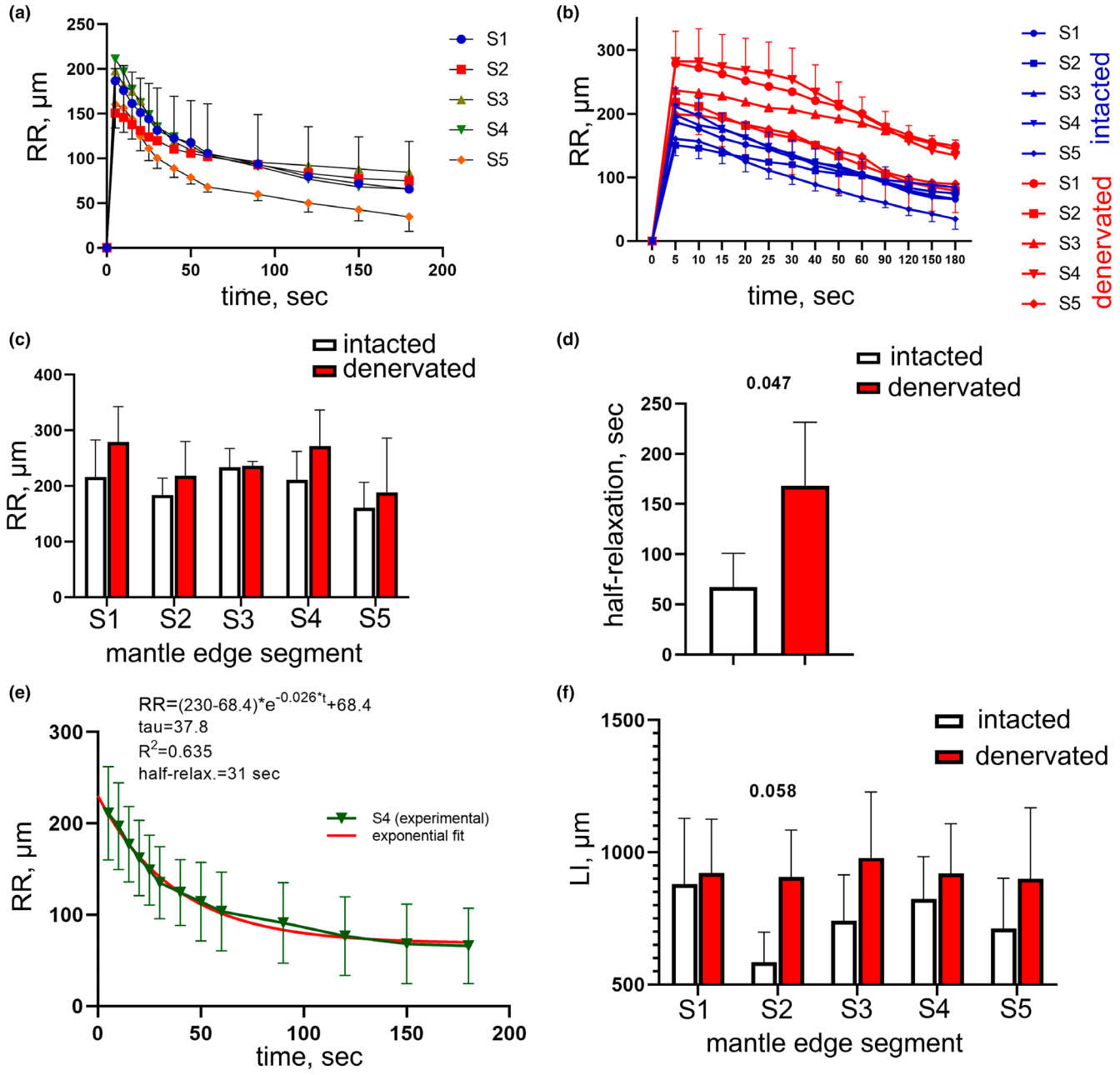

FIGURE 10 The characteristics of the retractile responses induced in the mantle by local mechanical stress. (a) A retraction and time decay of the retractile response (RR) registered in various segments (S1–S5, segment positions are shown by colour as in Figure 2) of the mantle edge of untreated (control) animals. (b) Time course of the retractile responses in untreated (blue) and denervated (red) animals. S1–S5, stimulated segments of the mantle edge. (c) Peak retractile response (RR at the 5th sec after mechanical stimulus application) for each stimulated mantle segment (S1–S5) in untreated (transparent) and denervated (red) animals. (d) The duration of the time interval required for a half-relaxation after retraction in untreated and denervated animals in segment 4. The exact *p*-value (nonparametric M–U test) is shown on the figure. (e) Representative curve for the decay phase of the RR (green) and a monoexponential regression curve (red) used for the calculation of half-relaxation time. (f) The magnitude of the lateral irradiation (LI) of the retractile responses observed in the untreated (transparent) and denervated (red) animals, calculated for each point on the mantle edge (S1–S5) as shown in Figure 2. The exact *p*-value (two-way ANOVA) is shown in the figure.

5.2 | Organization of the mantle nervous system

Our data reveal that the mantle nervous system of *H. psittacea* consists of numerous radial nerves that connect with a marginal nerve. This morphology is similar to that observed in linguliforms (Blochmann, 1900; Santagata, 2011) and craniiforms (Temereva, 2020, 2022). Before this study, the existence of a marginal nerve in rhynchonelliforms was debated (Hancock, 1858; Owen, 1853). However, our

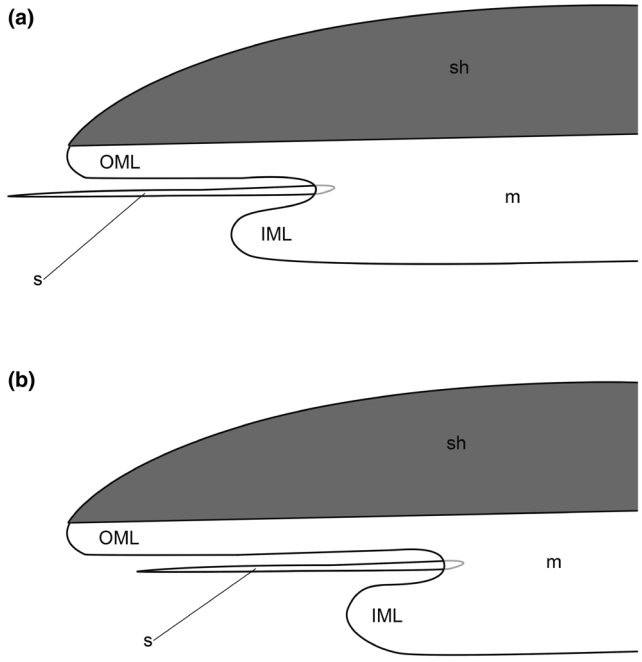

FIGURE 11 Scheme of mantle contraction in *Hemithiris psittacea*. (a) The relaxed mantle; (b) the contracted mantle. IML, inner mantle lobe; m, mantle; OML, outer mantle lobe; s, setae; sh, shell.

findings confirm the presence of a marginal nerve in rhynchonelliform brachiopods; its functional role is discussed in the following sections.

The fine structure of the mantle nerves in *H. psittacea* closely resembles that of the lophophoral nerves in brachiopods (Kuzmina & Temereva, 2021; Reed & Cloney, 1977; Temereva & Kuzmina, 2017, 2021; Williams et al., 1997). Most of the mantle nerves are located within the inner mantle epithelium. The supportive cells, which are modified epithelial cells, exhibit an elongated shape and possess basal processes containing intermediate filaments that attach to the basal lamina via hemidesmosomes. The cytoplasm of these cells is characterized by a well-developed rough endoplasmic reticulum and abundant glycogen granules. These supportive cells are similar to the radial glial cells found in various Bilateria groups (Alvarez-Buylla et al., 1987; Hartline, 2011; Mashanov et al., 2015; Helm et al., 2022; Beckers et al., 2019). They play a role in protecting nerve cells and supplying them with nutrients. The interepithelial positioning of nerve cells is likely a plesiomorphic trait for Bilateria (Kuzmina & Temereva, 2021). In the proximal parts of the radial nerves, we observed large perikarya with electron-lucent cytoplasm. The ultrastructure of these perikarya is similar to that of the large perikarya found in the lophophoral nerves and subenteric ganglion of brachiopods (Kuzmina & Temereva, 2021; Temereva & Kuzmina, 2021), as well as the motor neurons in the dorsal ganglion of phoronids (Temereva, 2017; Temereva & Malakhov, 2009). Our study revealed two types of neurites in the mantle nerves of *H. psittacea*, which are consistent with data on the structure of the subenteric ganglion of *Coptothyris grayi* (Kuzmina & Temereva, 2021) and the nervous system of the lophophore in *C. grayi* (Temereva & Kuzmina, 2021).

Additionally, we observed rare nerves in the outer epithelium and connective tissue of the mantle. The nerves within the connective tissue are surrounded by a basal lamina. Similar nerves in connective tissue have been described in the lophophore of various brachiopod groups (Williams et al., 1997; Temereva & Tsitrin, 2015; Kuzmina & Temereva, 2022; Temereva & Kuzmina, 2017, 2021; Temereva, 2022).

Our study is the first to identify collar receptor cells located near the setal follicle in adult brachiopods. A similar sensory complex, consisting of a receptor cell and a seta, has been previously described in rhynchonelliform larvae (Lüter, 2001, 2007).

5.3 | Morpho-functional analysis of the muscular and nervous systems of the mantle

In the present study, the role of mantle innervation in controlling mantle retraction and setae extension in brachiopods was functionally tested for the first time. It has been shown that in the resting state, the inner mantle lobe is retracted, and the distance from the mantle edge to the shell margin varies insignificantly across all sectors of the mantle. Denervation resulted in the relaxation of the mantle edge and a reduction of the RD. The relaxation induced by denervation suggests that the mantle exhibits a pre-retracted state. This state is possibly mediated by a permanent efferent firing of the mantle nerves, causing tonic contraction of the muscular fibres of the mantle, and may be controlled by the subenteric ganglion. It is known that the serial mantle muscles extend near the setal follicles. Additionally, the proximal part of each seta interacts with a cilium of the sensory cell embedded in the epithelium in proximity to the setae. These structural peculiarities suggest that the pre-retracted state aims to minimize spontaneous low-amplitude dorso-ventral wavering of the setae caused by water flow. Thus, mantle edge pre-retraction may facilitate sensory selectivity of the sensory complexes of setae and collar receptors by suppressing non-significant signals and amplifying physiologically valuable mechanical signals.

Also, mechanically induced contractile responses of the mantle edge were registered and analysed in intact and denervated animals for the first time in the present investigation. The rapid closure of the shell valves is a natural

defence response in brachiopods to mechanical stimuli (Peck et al., 1997). This defensive reflex is achieved through the generalized retraction of the mantle, followed by the contraction of the adductor muscles, which extend from the ventral to the dorsal valves. For this function to be successful, it is essential to synchronize and integrate the contractions of both the mantle musculature and the adductors. It can be hypothesized that the radial mantle nerves play a role in coordinating mantle retraction with valve closure.

Our experiments have revealed that the mantle edge is able to respond actively not only by generalized contraction but also by a reversible, highly localized retraction. This localized retractile response is comparable in magnitude to the length of the setae and is accompanied by restricted irradiation. The magnitude of the retraction and lateral irradiation allow us to hypothesize that the local response is a protective mechanism aimed at preserving setae integrity in cases of damaging mechanical impacts (Figure 11).

Our experiments revealed that denervation causes a delay in post-contractile relaxation and expansion of irradiation. These observations suggest that the innervation of the mantle edge, which connects to the subenteric ganglion, is complex and plays a role beyond generalized defensive retraction. Mantle innervation may restrict contraction and the generalisation of local mechanically induced retraction, that is, LI. After local mechanical stimulation, the mantle's nervous system inhibits a generalized contraction, resulting in only a restricted contraction of the mantle. Speculatively, the intensively developed marginal and radial nerves may be involved in the control of retractile irradiation.

Finally, our experiments demonstrated the preservation of mantle contractile responses in denervated animals. These results suggest the possibility of an autonomous, that is, independent of excitatory influences from the subenteric ganglion, contractile response and retraction of the mantle edge. An autonomous response could be mediated through two neuronal mechanisms: an axon reflex, which is carried out via radial mantle nerves, or the transmission of excitation through a marginal mantle nerve.

Since no direct contacts between muscle and nerve cells were found, we speculate that muscle cell activation occurs in the classical way as a result of the induced secretion of neurotransmitters into the extracellular matrix rather than by electrotonic transmission through gap junctions.

6 | CONCLUSION

The soft body of brachiopods is protected by a mineralized shell with valves that close tightly when the organism is threatened. The mantle lining this shell serves as the primary sensory organ, particularly at its margin, which is fringed with setae that come into contact with the environment during filtration when the valves are open. The mantle's neuromuscular system is responsible for the reflex response to external stimulation, leading to the retraction of the mantle edge and closure of the shell valves for protection. We found that the main sensitive elements of the mantle of the brachiopod *H. psittacea* are the sensory complex of the setae and collar receptor. The mantle is innervated by a pair of main mantle nerves that arise from the subenteric ganglion. The mantle nerve system consists of numerous radial nerves and a thick marginal nerve, which are located intraepithelially. Mantle retraction is caused by the contraction of serial longitudinal mantle muscles. We demonstrated that mantle contraction can occur independently of the central nervous system, although the subenteric ganglion plays a role in retaining the mantle in a pre-contracting state during rest to facilitate sensory selectivity of the sensory complexes of setae.

ACKNOWLEDGEMENTS

The study is supported by Russian Science Foundation (#23-14-00020). The research was performed at the User Facilities Center of M.V. Lomonosov Moscow State University. We are pleased to thank A. Petrenko for help with design of the experimental chamber for physiological experiments.

CONFLICT OF INTEREST STATEMENT

The authors declare that there is no conflict of interest.

DATA AVAILABILITY STATEMENT

The original contributions presented in the study are included in the article; further inquiries can be directed to the corresponding author.

ORCID

Anna V. Ratnovskaya https://orcid.org/0000-0001-5155-4597

REFERENCES

Altenburger, A., & Wanninger, A. (2009). Comparative larval myogenesis and adult myoanatomy of the rhynchonelliform (articulate) brachiopods *Argyrotheca cordata*, *A. cistellula*, and *Terebratalia transversa*. *Frontiers in Zoology*, *6*(1), 1–14.

Altenburger, A., & Wanninger, A. (2010). Neuromuscular development in *Novocrania anomala*: Evidence for the presence of serotonin and a spiralian-like apical organ in lecithotrophic brachiopod larvae. *Evolution & Development*, *12*(1), 16–24.

Alvarez-Buylla, A., Buskirk, D. R., & Nottebohm, F. (1987). Monoclonal antibody reveals radial glia in adult avian brain. *Journal of Comparative Neurology*, *264*(2), 159–170.

Beckers, A., Van Dyck, A., Bollaerts, I., Van Houcke, J., Lefevere, E., Andries, L., & Moons, L. (2019). An antagonistic axon-dendrite

interplay enables efficient neuronal repair in the adult zebrafish central nervous system. *Molecular Neurobiology*, *56*, 3175–3192.

Blochmann, F. (1900). Untersuchungen über den Bau der Brachiopoden. In *Pt. 2. Die Anatomie von Discinisca lamellosa (Broderip) und Lingula anatina (Bruguiére)*. Gustav Fischer.

Carlson, S. J. (2016). The evolution of Brachiopoda. *Annual Review of Earth and Planetary Sciences*, *44*(1), 409–438.

Hancock, A. (1858). XXXIV. On the organization of the brachiopoda. *Philosophical Transactions of the Royal Society of London*, *148*, 791–869.

Hartline, D. K. (2011). The evolutionary origins of glia. *Glia*, *59*(9), 1215–1236.

Helm, C., Schwarze, G., & Beckers, P. (2022). Loss of complexity from larval towards adult nervous systems in Chaetopteridae (Chaetopteriformia, Annelida) unveils evolutionary patterns in Annelida. *Organisms Diversity & Evolution*, *22*(3), 631–647.

Kuga, H., & Matsuno, A. (1988). Ultrastructural investigations on the anterior adductor muscle of a brachiopoda, *Lingula unguis*. *Cell Structure and Function*, *13*(4), 271–279.

Kuzmina, T., & Temereva, E. (2021). Ultrastructure of ganglia in the brachiopod *Coptothyris grayi* and its phylogenetic significance. *Journal of Zoological Systematics and Evolutionary Research*, *59*(2), 376–386.

Kuzmina, T., & Temereva, E. (2022). Tentacle muscles in brachiopods: Ultrastructure and relation to peculiarities of life style. *Journal of Experimental Zoology Part B: Molecular and Developmental Evolution*, *338*(3), 192–208.

Lüter, C. (2001). Brachiopod larval setae—a key to the phylum's ancestral life cycle? In *Brachiopods* (pp. 60–69). CRC Press.

Lüter, C. (2007). Treatise on invertebrate paleontology, part H, Brachiopoda (revised). *Boulder, Colorado and Lawrence, Kansas: Geological Society of America and the University of Kansas*, *6*, 423–440.

Malakhov, V. V., Kuzmina, T. V., & Madison, A. A. (2021). Classification of planktonic stages of extant brachiopods. *Invertebrate Zoology*, *18*(2), 95–104.

Mashanov, V. S., Zueva, O. R., & García-Arrarás, J. E. (2015). Heterogeneous generation of new cells in the adult echinoderm nervous system. *Frontiers in Neuroanatomy*, *9*, 123.

Owen, P. (1853). On the anatomy of *Terebratula*. In T. Davidson, P. Owen, P. Carpenter, & T. Davidson (Eds.), *British fossil Brachiopoda. Vol. I. With a general introduction* (pp. 1–136). Monographs of the Palaeontographical Society.

Peck, L. S., Rhodes, M. L., Curry, G. B., & Ansell, A. D. (1997). Physiology. In R. L. Kaesler (Ed.), *Treatise on invertebrate paleontology, part H, brachiopoda (revised). Volume 1: Introduction* (pp. 213–240). University of Kansas Press.

Reed, C. G., & Cloney, R. A. (1977). Brachiopod tentacles: Ultrastructure and functional significance of the connective tissue and myoepithelial cells in *Terebratalia*. *Cell and Tissue Research*, *185*, 17–42.

Rudwick, M. J. S. (1970). *Living and fossil brachiopods* (p. 199). Hutchinson and Co. Ltd.

Santagata, S. (2011). Evaluating neurophylogenetic patterns in the larval nervous systems of brachiopods and their evolutionary significance to other bilaterian phyla. *Journal of Morphology*, *272*(10), 1153–1169.

Storch, V., & Welsch, U. (1976). Elektronenmikroskopische und enzymhistochemische Untersuchungen über Lophophor und Tentakeln von *Lingula unguis* L. (Brachiopoda). Zoologische Jahrbücher. *Abteilung für Anatomie Und Ontogenie der Tiere*, *96*, 225–237.

Temereva, E. (2022). First modern data on the lophophore nervous system in adult *Novocrania anomala* and a current assessment of brachiopod phylogeny. *Biology*, *11*(3), 406.

Temereva, E. N. (2017). Innervation of the lophophore suggests that the phoronid *Phoronis ovalis* is a link between phoronids and bryozoans. *Scientific Reports*, *7*(1), 14440.

Temereva, E. N. (2020). First data on the organization of the nervous system in juveniles of *Novocrania anomala* (Brachiopoda, Craniiformea). *Scientific Reports*, *10*(1), 9295.

Temereva, E. N., & Kuzmina, T. V. (2017). The first data on the innervation of the lophophore in the rhynchonelliform brachiopod *Hemithiris psittacea*: What is the ground pattern of the lophophore in lophophorates? *BMC Evolutionary Biology*, *17*, 1–19.

Temereva, E. N., & Kuzmina, T. V. (2021). The nervous system of the most complex lophophore provides new insights into the evolution of Brachiopoda. *Scientific Reports*, *11*(1), 16192.

Temereva, E. N., & Malakhov, V. V. (2009). Microscopic anatomy and ultrastructure of the nervous system of *Phoronopsis harmeri* Pixell, 1912 (Lophophorata: Phoronida). *Russian Journal of Marine Biology*, *35*, 388–404.

Temereva, E. N., & Tsitrin, E. B. (2015). Modern data on the innervation of the lophophore in *Lingula anatina* (Brachiopoda) support the monophyly of the lophophorates. *PLoS One*, *10*(4), e0123040.

Williams, A., Carlson, S. J., Brunton, C. H. C., Holmer, L. E., & Popov, L. (1996). A supra-ordinal classification of the Brachiopoda. *Philosophical Transactions of the Royal Society of London. Series B: Biological Sciences*, *351*(1344), 1171–1193.

Williams, A., James, M. A., Emig, C. C., Mackay, S., & Rhodes, M. C. (1997). Anatomy. In R. L. Kaesler (Ed.), *Treatise on invertebrate paleontology, part H, brachiopoda (revised). Volume 1: Introduction* (pp. 7–188). University of Kansas Press.

How to cite this article: Ratnovskaya, A. V., Kuzmina, T. V., & Kuzmin, V. S. (2025). Morpho-functional analysis of musculature and nervous system of mantle in brachiopod *Hemithiris psittacea* (Gmelin, 1791). *Acta Zoologica*, *00*, 1–14. https://doi.org/10.1111/azo.12548